Mesoscale Eddy–Internal Wave Coupling. Part II: Energetics and Results from PolyMode

KURT L. POLZIN

Woods Hole Oceanographic Institute, Woods Hole, Massachusetts

(Manuscript received 29 April 2008, in final form 5 October 2009)

ABSTRACT

The issue of internal wave–mesoscale eddy interactions is revisited. Previous observational work identified the mesoscale eddy field as a possible source of internal wave energy. Characterization of the coupling as a viscous process provides a smaller horizontal transfer coefficient than previously obtained, with $\nu_h \cong 50\ \mathrm{m^2\ s^{-1}}$ in contrast to $\nu_h \cong 200$–$400\ \mathrm{m^2\ s^{-1}}$, and a vertical transfer coefficient bounded away from zero, with $\nu_v + (f^2/N^2)K_h \cong 2.5 \pm 0.3 \times 10^{-3}\ \mathrm{m^2\ s^{-1}}$ in contrast to $\nu_v + (f^2/N^2)K_h = 0 \pm 2 \times 10^{-2}\ \mathrm{m^2\ s^{-1}}$. Current meter data from the Local Dynamics Experiment of the PolyMode field program indicate mesoscale eddy–internal wave coupling through horizontal interactions (i) is a significant sink of eddy energy and (ii) plays an $O(1)$ role in the energy budget of the internal wave field.

1. Introduction

a. Preliminaries

Winds and air–sea exchanges of heat and freshwater are ultimately responsible for the basin-scale currents or general circulation of the oceans. To achieve a state where the energy and enstrophy (vorticity squared) of the ocean is not continuously increasing, some form of dissipation is required to balance this forcing. Although the previous statement may seem obvious, little is known about how and where this dissipation occurs.

Early theories of the wind driven circulation (Stommel 1948; Munk 1950) view the western boundary as a region where energy and vorticity input by winds in midgyre could be dissipated. Apart from rationalizing why western boundary currents are located on the western boundary, even the crudest perusal of observations suggests distinct discrepancies with such models. One example is that an intensely energetic mesoscale eddy field is associated with the Gulf Stream after its separation (e.g., Schmitz 1976) with the perception (Moore 1963) that one reason for the existence of such an intense eddy field is insufficient dissipation at the boundary. Thus, the question of closing an energy budget for the general circulation (e.g., Wunsch and Ferrari 2004) is to remove dissipation from the mean budget and place it in the eddy budget. One can follow the thread and ask, ''how does the mesoscale eddy field dissipate?'' Among many possible mechanisms (Ferrari and Wunsch 2009) is the exchange of energy between the mesoscale eddy field and the internal wave field. The rest of this introduction attempts to discuss the phenomenology of mesoscale eddy–internal coupling, review previous results, and lay groundwork for the rest of the paper.

b. Mesoscale eddy–internal wave coupling

A cornerstone of theoretical understanding for wave problems concerns zonal-mean theory and the analysis of wave propagation in parallel shear flows. A basic constraint, typically referred to as Andrews and McIntyre's generalized Eliassen–Palm (EP) flux theorem (Andrews and McIntyre 1976),

$$\frac{dk\mathcal{A}}{dt} + \nabla \cdot \mathbf{F} = \mathcal{D} + O(\alpha^3), \tag{1}$$

states that in the absence of dissipation $\mathcal{D}$ and nonlinearity (small wave amplitude α limit) and for steady conditions, the Eliassen–Palm flux $\mathbf{F}$ is spatially nondivergent: $\nabla \cdot \mathbf{F} = 0$. In terms of either linear internal wave or linear Rossby wave kinematics, the Eliassen–Palm flux $\mathbf{F} = k\mathbf{C}_g\mathcal{A}$, with streamwise (zonal) wavenumber k, group velocity $\mathbf{C}_g$, and wave action $\mathcal{A}$. With

Corresponding author address: Kurt L. Polzin, WHOI, MS#21, Woods Hole, MA 02543.
E-mail: kpolzin@whoi.edu

DOI: 10.1175/2009JPO4039.1

respect to the mean fields, the attendant nonacceleration theorem (Andrews et al. 1987) states that the mean flow remains steady if $\nabla \cdot \mathbf{F} = 0$.

This cornerstone summarizes a vast literature about waves in zonal or symmetric mean flows. In this restricted paradigm, the EP flux (equivalently, the pseudomomentum flux or wave stress) assumes a primary role, as it should because of the attendant nonacceleration theorems. However, there is something much more general than pseudomomentum flux conservation in symmetric flows, and this is action conservation, which is independent of the spatial structure of the background flow field. The intent of this work is to demonstrate that, if one drops the assumption of mean state spatial symmetry inherent in the EP flux theorem, mesoscale eddies and internal waves are coupled through a linear wave stress–eddy rate of strain relation, which leads to the representation of internal wave effects as an eddy viscosity.

1) SYMMETRY

A convenient starting place to examine eddy–wave coupling in three dimensions (3D) is to invoke a decomposition of the velocity [$\mathbf{u} = (u, v, w)$], buoyancy ($b = -g\rho/\rho_o$ with gravitational constant g and density ρ), and pressure (π) fields into a quasigeostrophic mean ($^-$) and small-amplitude internal wave ($''$) perturbations on the basis of a time scale separation: $\phi = \overline{\phi} + \phi''$ with $\overline{\phi} = \tau^{-1}\int_0^\tau \phi\, dt$, in which τ is much longer than the internal wave time scale but smaller than the eddy time scale. The double prime notation for internal wave field variables is retained for consistency with a companion paper (K. L. Polzin 2009, unpublished manuscript).

Employing this averaging process to the equations of motion returns the result that the right-hand side of the mean equations represents the flux divergence of pseudomomentum. Following Müller (1976), the wave stress S_{ij} acting as a source term acting on the mean fields is

$$S_{ij} = \int d\mathbf{k}\, n(\mathbf{k}, \mathbf{x}, t) k^i C_g^j, \tag{2}$$

with 3D wave action spectrum $n \equiv E/\omega$, intrinsic frequency $\omega = \sigma - \mathbf{k} \cdot \overline{\mathbf{u}}$, group velocity $\mathbf{C}_g$, wave vector $\mathbf{k} = (k, l, m)$ having horizontal magnitude $k_h = (k^2 + l^2)^{1/2}$, and energy density $E = E_k + E_p$. The wave stress (2) is readily identified as a pseudomomentum flux and is a generalization of the Eliassen–Palm flux $\mathbf{F}$ in (1). This formulation assumes a slowly varying plane wave solution and manipulations involving the algebraic factors relating (u'', v'', w'', b'', and π'') for linear internal waves.

A key insight is that pseudomomentum is not, in general, conserved in a wave–mean interaction problem (Bühler and McIntyre 2005; Polzin 2008). For steady conditions, small-amplitude waves in a slowly varying background have a nondivergent action flux,

$$\int d\mathbf{k}\, \nabla \cdot \mathbf{C}_g n = 0; \tag{3}$$

with a spatial scale separation between wave and background, the evolution of a wave vector following a wave packet is given by the ray equations:

$$\begin{aligned} \frac{dk}{dt} &= -k\overline{u}_x - l\overline{v}_x - m\overline{w}_x, \\ \frac{dl}{dt} &= -k\overline{u}_y - l\overline{v}_y - m\overline{w}_y, \quad \text{and} \\ \frac{dm}{dt} &= -k\overline{u}_z - l\overline{v}_z - m\overline{w}_z. \end{aligned} \tag{4}$$

In a zonally oriented parallel shear flow, the streamwise component k of the horizontal wave vector is constant following the ray trajectory. Thus, $\nabla \cdot \mathbf{F} = \nabla_j \cdot S_{x,j} = \int d\mathbf{k}\, k\nabla \cdot \mathbf{C}_g n = 0$ (the gradient operator contracts with $\mathbf{C}_g$) and the Eliassen–Palm flux theorem (1) is nothing more than an action flux conservation statement.

It is from this vantage point that one can appreciate that the generalized Eliassen–Palm flux theorem does not apply to asymmetric (3D) flows. If the background velocity field contains horizontal gradients in both (x, y) dimensions, the streamwise component of the horizontal wave vector evolves following a ray trajectory and thus the pseudomomentum flux is generally divergent. A simple rationalization of the difference in behavior between 2D (symmetric) and 3D (asymmetric) systems comes from theoretical physics: each symmetry exhibited by a Hamiltonian system corresponds to a conservation principle (Nöther's theorem; e.g., Shepherd 1990). For spatial symmetries, the conservation principle concerns momentum: axisymmetric flows preserve the flux of pseudomomentum in the symmetric coordinate.

2) ASYMMETRY, THE SHRINKING CATASTROPHE, AND WAVE CAPTURE

It turns out that the filamentation of waves by a rate of strain field provides the essential mechanism through which the streamwise wavenumber varies and streamwise pseudomomentum is not conserved. Bühler and McIntyre (2005) point to an analogy between internal wave propagation in horizontally nondivergent flows and the problem of particle pair separation in incompressible 2D turbulence. In this relative dispersion problem, particle pairs undergo exponential separation when the rate of strain variance exceeds relative vorticity variance:

$$S_s^2 + S_n^2 > \zeta^2, \tag{5}$$

with $S_s \equiv \overline{v}_x + \overline{u}_y$ being the shear component of the strain rate, $S_n \equiv \overline{u}_x - \overline{v}_y$ being the normal component, and $\zeta \equiv \overline{v}_x - \overline{u}_y$ being relative vorticity (Polzin 2008). Equation (5) is simply the Okubo–Weiss criterion (e.g., Provenzale 1999). Bühler and McIntyre (2005) argue that the problem of small-amplitude waves in a horizontally nondivergent flow field is kinematically similar to particle pair separation under the hypothesis of a scale separation. In this case, the ray equations of (4) have solutions

$$\mathbf{k} \propto e^{\pm(S_n^2 + S_s^2 - \zeta^2)^{1/2} t/2}. \tag{6}$$

Thus, a dominance of rate of strain variance over relative vorticity variance leads to an exponential increase/decrease in the density of phase lines: that is, an exponential increase/decrease in horizontal wavenumber, $k_h = (k^2 + l^2)^{1/2}$ (Fig. 1). Vorticity simply tends to rotate the horizontal wave vector (k, l) in physical space. This provides a simple picture of pseudomomentum flux divergence associated with an internal wave packet interacting with an eddy rate of strain.

Bühler and McIntyre (2005) further argue for a scenario, which they term "wave capture" and Jones (1969) labels a "shrinking catastrophe." Simply put, the vertical wavenumber is slaved to the horizontal wavenumber, $dm/dt = -k\overline{u}_z - l\overline{v}_z$, so that exponential growth of the horizontal wavenumber implies exponential growth or decay of vertical wavenumber in the presence of thermal wind shear. Those waves with growing vertical wavenumber will tend to be trapped (captured) within the extensive regions of the eddy strain field. In two dimensions, the zonal wavenumber is constant and the meridional wavenumber grows linearly in time. The vertical wavenumber also experiences linear growth but is decoupled from the evolution of the horizontal component. In two dimensions, one has the notion of a critical layer condition $\sigma - k\overline{u} = \pm f$ as the intrinsic frequency approaches the lower bound for freely propagating waves f (f is the Coriolis parameter). Such critical layers are not a part of the phenomenology in three dimensions.

The ray-tracing arguments about internal wave packets interacting with mesoscale eddies return useful pictures about a mechanism, but they do not provide information about the net transfer rates for the observations. This requires consideration of the energy balance, which is done later within the quasigeostrophic limit. Note that quasigeostrophy invokes both a smallness of Rossby number and that the two horizontal length scales are similar. It is this last assumption that is crucial to scaling the horizontal divergence as O(Rossby number squared): that is, crucial to the statement that the background field is horizontally nondivergent in the context of ray tracing (4) and its summary in (5) and (6). The length scale requirement of quasigeostrophy further underscores the issue of how asymmetry in the background influences the character of the wave–mean interaction.

c. Linearized wave energy balances

The internal wave energy equation is (Müller 1976)

$$\begin{aligned}\left(\frac{\partial}{\partial t} + \overline{u}\cdot\nabla_h\right)(E_k + E_p) + \nabla\cdot\overline{\pi''\mathbf{u}''} \\ = -\overline{u''u''}\,\overline{u}_x - \overline{u''v''}\,\overline{u}_y - \overline{u''w''}\,\overline{u}_z - \overline{v''u''}\,\overline{v}_x - \overline{v''v''}\,\overline{v}_y \\ - \overline{v''w''}\,\overline{v}_z - N^{-2}\overline{b''u''}\,\overline{b}_x - N^{-2}\overline{b''v''}\,\overline{b}_y,\end{aligned} \tag{7}$$

with kinetic $[E_k = (u''^2 + v''^2 + w''^2)/2]$ and potential $[E_p = (N^{-2}b''^2)/2]$ energies. Temporal variability and advection of internal wave energy by the geostrophic velocity field are balanced by wave propagation and energy exchanges between the quasigeostrophic and internal wave fields. Nonlinearity and dissipation are assumed to be higher-order effects. With the exception of vertical buoyancy fluxes $\overline{b''w''}$, which are negligible for linear waves, the energy exchanges are adiabatic. Similarly, spatial gradients of the vertical velocity $\overline{w}$ do not appear, because $\overline{w}_z$ is small (order Rossby number squared) in the quasigeostrophic approximation. The thermal wind relation can be invoked to cast the vertical Reynolds stress and horizontal buoyancy flux as the rate of work by an effective vertical stress acting on the vertical gradient of horizontal momentum:

$$\overline{u''w''}\,\overline{u}_z + N^{-2}\overline{b''v''}\,\overline{b}_y = \left(\overline{u''w''} - \frac{f}{N^2}\overline{b''}\,\overline{v''}\right)\overline{u}_z \quad \text{and}$$

$$\overline{v''w''}\,\overline{v}_z + N^{-2}\overline{b''u''}\,\overline{b}_x = \left(\overline{v''w''} + \frac{f}{N^2}\overline{b''}\,\overline{u''}\right)\overline{v}_z.$$

These two terms in the effective stress will cancel each other in the limit that $\omega \to f$ (Ruddick and Joyce 1979).

The character of the horizontal terms for quasigeostrophic flows can be made more apparent by expressing the right-hand side of (7) as

$$-\overline{u''u''}\,\overline{u}_x - \overline{v''v''}\,\overline{v}_y = -(\overline{u''u''} - \overline{v''v''})S_n/2$$

$$-\overline{u''v''}\,\overline{u}_y - \overline{v''u''}\,\overline{v}_x = -\overline{u''v''}S_s.$$

Within the wave capture scenario, linear wave kinematics implies a negative stress–strain correlation for internal waves (i.e., a positive horizontal viscosity in a flux-gradient closure) and a positive stress–strain correlation

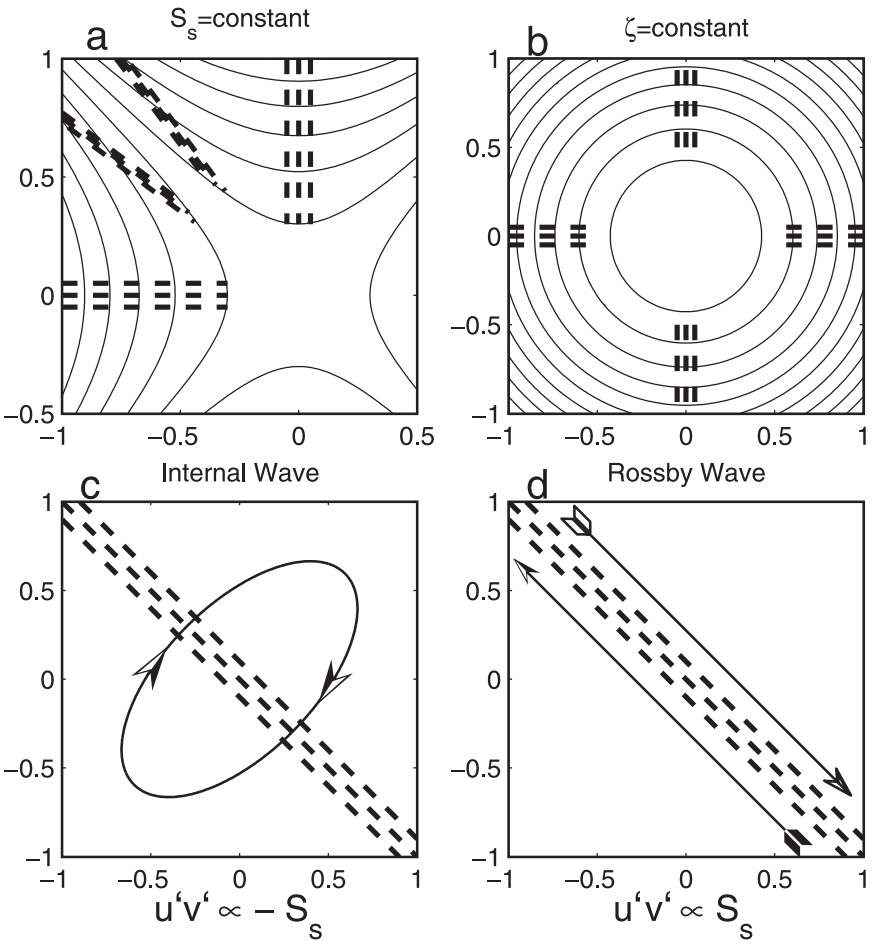

FIG. 1. Phase lines (dashed) of waves being passively advected by two realizations of a steady mean flow having streamlines denoted by the solid contours: (a) a spatially constant shear strain S_s and (b) a spatially constant relative vorticity ζ. (c) For internal waves, parcel velocities projected onto the horizontal plane (see arrows) are elliptically polarized with the major axis parallel to the horizontal wave vector and normal to wave crests (lines of constant phase). (d) For Rossby waves, the horizontal velocity trace is linearly polarized (see arrows) and parallel to wave crests (lines of constant phase). (c),(d) The tendency of background rate of strain to create anisotropic wave fields and wave stresses by preferentially orienting the phase lines along the extensive axis of a strain field can be inferred. However, there is an important distinction in the two cases. Parameterization of the stress–strain relation in terms of a flux-gradient relation leads to a positive eddy viscosity for internal waves and a negative eddy viscosity for Rossby waves. (b) The tendency of vorticity to not result in wave stresses can also be inferred.

for Rossby waves (i.e., a negative horizontal viscosity; Fig. 1). For internal waves, the negative correlation follows from the fact that the major axis of the horizontal velocity trace is parallel to the projection of the wave vector onto the horizontal plane. For Rossby waves, geostrophy implies that the horizontal velocity is normal to the horizontal wave vector. Upgradient transfers (a negative viscosity) have long been recognized as a property of many different planetary scale systems (Starr 1968).

Two further points are to be made. First, the right-hand side of (7) represents the rate at which the pseudomomentum flux (2) is doing work against mean gradients. It is thus a description of how internal wave energy is altered through wave radiation (work and an energy flux divergence). Exchanges of energy through the vertical terms can be either positive or negative, depending on the sign of the vertical group velocity, horizontal wavenumbers, and vertical shear. The standard parallel shear flow critical layer has, with $\overline{u}_z > 0$, $C_g^z < 0$, and $k < 0$,

$\sigma - k\bar{u} \to f$ and the wave loses energy. The energetics of a wave capture event admits to a similar characterization in the vertical coordinate. However, despite the theoretical attention that has been paid to the low-frequency limit, the observations indicate that the net energy exchange in the vertical coordinate is dominated by high-frequency waves. Second, the horizontal coupling can be written as the product of a momentum flux and the rate of strain tensor, just as one would in the context of isotropic turbulence (e.g., Tennekes and Lumley 1972). Thus, in this wave problem, the filamentation of a wave by a larger-scale background described in the previous subsection plays a role analogous to turbulent energy transfer by vortex stretching.

If closure of mesoscale eddy–internal wave coupling through flux–gradient relations can be justified, in which $-2\overline{u''v''} = \nu_h(\bar{v}_x + \bar{u}_y)$, $-\overline{u''w''} = \nu_v \bar{u}_z$, $-\overline{u''u''} = \nu_h \bar{u}_x$, $-\overline{v''v''} = \nu_h \bar{v}_y$, $-\overline{u''b''} = K_h \bar{b}_x$, and $-\overline{v''b''} = K_h \bar{b}_y$, then considerable simplification results. The right-hand side of the internal wave energy equation becomes, after a little manipulation, a simple source term:

$$S_o = \nu_h(\bar{v}_x^2 + \bar{v}_y^2 + \bar{u}_x^2 + \bar{u}_y^2) + \left(\nu_v + \frac{f^2}{N^2}K_h\right)(\bar{u}_z^2 + \bar{v}_z^2). \tag{8}$$

d. Observations

It remains to inquire whether the coupling is sufficiently large that interior damping of the mesoscale is considered an important process. The first step is a characterization of the magnitude of the coupling, which has been investigated observationally using current meter data from moored arrays bracketing the Gulf Stream. This includes individual moorings at site D (39°N, 70°W), arrays at (28°N, 70°W) [the MidOcean Dynamics Experiment (MODE), the Internal Wave Experiment (IWEX), and the Local Dynamics Experiment (LDE; 31°N, 69°30′W) component of PolyMode], and individual moorings that were part of PolyMode arrays I (35°–36°N, 55°W) and II (28°N, 56°W and 28°N, 65°W).

Frankignoul (1974) reports horizontally anisotropic conditions at high frequencies to be associated with large mean currents (site D) and correlation between $u''^2 - v''^2$ and $\bar{u}_x - \bar{v}_y$ (MODE-0). Using data from MODE, Frankignoul (1976) reports 1) $\nu_h = O(10\text{–}1000)$ m^2 s^{-1}, using direct estimates of $\overline{u''v''}$ versus $(\bar{v}_x + \bar{u}_y)$ and of $u''^2 - v''^2$ versus $(\bar{u}_x - \bar{v}_y)$, and 2) $\nu_v + (f^2/N^2)K_h \leq O(0.1\ \text{m}^2\ \text{s}^{-1})$ from correspondences between fluctuations of E and $\bar{u}_z^2 + \bar{v}_z^2$. The latter estimates of vertical coupling are refined using data from IWEX to be $|\nu_v + (f^2/N^2)K_h| \leq O(0.01\ \text{m}^2\ \text{s}^{-1})$. Frankignoul and Joyce (1979) and Ruddick and Joyce (1979) interpret data from PolyMode I and II as an effective eddy viscosity of $\nu_v + (f^2/N^2)K_h = 0 \pm 2 \times 10^{-2}$ m^2 s^{-1}. Finally, Brown and Owens (1981) use direct estimates of $-2\overline{u''v''}$ regressed against $(\bar{v}_x + \bar{u}_y)$ to obtain $\nu_h = 200\text{–}400$ m^2 s^{-1} (PolyMode LDE).

e. Forward

The problem of wave forcing of the oceanic general circulation is much richer than is to be inferred from taking the EP flux theorem (1) at face value and assuming an adiabatic limit. A key contribution of this work is the recognition of the role that asymmetry and strain play in the phenomenology, energetics, and dynamics of wave–mean interactions. Note that strain is not regarded as such until Bühler and McIntyre (2005).

The purpose of this paper is to review the previous calculations of horizontal (section 2) and vertical (section 3) coupling and to place those estimates into the context of the Bryden (1982) LDE eddy energy budget (section 4). A summary and discussion concludes the paper. A companion paper (K. L. Polzin 2009, unpublished manuscript) examines dynamical issues and the LDE potential enstrophy budget.

2. Horizontal coupling

Brown and Owens (1981) present a scatterplot of horizontal stress $\overline{u''v''}$ versus $\bar{v}_x + \bar{u}_y$ using data from a current meter array deployed during the LDE of the PolyMode program. The LDE array is likely the most appropriate dataset for such a study. The array was deployed for 15 months and consisted of two crosses centered about a central mooring located at 31°N, 69°30′W. The inner cross moorings had a nominal spacing of 25 km because the array was designed to resolve mesoscale velocity gradients. These moorings were instrumented with current meters at two levels, at 600- and 825-m water depth. The outer moorings were instrumented with a single current meter at 600-m depth and had a larger horizontal spacing. Only the inner cross data are used here. Instrument failures limit estimation of relative vorticity and rate of strain to involving the center, northeast, northwest and southwest mooring over the full 15-month deployment period at the 825-m level. For estimates involving both vertical and horizontal gradients, estimates are available from the center–northwest–northeast triangle for a 225-day period.

The analysis presented here is similar, though not identical, to Brown and Owens in the following: First, data from the center, northeast, northwest, and southwest moorings of the LDE inner cross at 825 m are used

for the internal wave estimates, and mesoscale gradients are estimated as first differences using the two possible triangles. Brown and Owens included data from the shorter (108 day) southeast current meter record and estimated the mesoscale gradients from centered differences when possible. Second, Brown and Owens defined the internal wave band with a filter having a half power point at $0.8f$. Here, mesoscale velocity gradients are defined by a low-pass filter with ½ power at 10-day periods and the high-frequency data are detrended. A filter having a 2-day ½ power point has also been used. No appreciable differences were noted. Finally, Brown and Owens estimate the $\overline{u''v''}$ cospectrum $C_{u,v}$ with four-day piece length transform intervals. A transform interval of 1024 points (equivalent to 11 inertial periods at 15-min sampling) is used here.

The major stated difference is that Brown and Owens estimate the horizontal stress as $\int_{2f}^{N}[(\omega^2 - f^2)/(\omega^2 + f^2)] \times C_{u,v}(\omega)\, d\omega$. Multiplication of the stress estimate by the transfer function $(\omega^2 - f^2)/(\omega^2 + f^2)$ is appropriate only for the vertical stress estimate, in which there is a cancelation between the Reynolds stress $\overline{u''w''}$ and the buoyancy flux, $\overline{v''b''}$ (Ruddick and Joyce 1979).

My regression of $\overline{u''v''}$ versus S_s returns a horizontal viscosity estimate of $\nu_h \cong 64 \pm 20$ m^2 s^{-1}, which is significantly smaller than the Brown and Owens estimate of $4(\pm 1) \times 10^2$ m^2 s^{-1} at 825 m. Consequently, regressions between $\int(P_{u,u} - P_{v,v})\, d\sigma$ versus S_n and $\int(P_{u,u} + P_{v,v})\, d\sigma$ versus ζ are both investigated (Fig. 2), in which $P_{x,x}$ represents the power spectrum of x''. The results are consistent with the expectation for a flux–gradient closure: the $\int(P_{u,u} - P_{v,v})\, d\sigma$ versus S_n regression results in $\nu_h \cong 37 \pm 16$ m^2 s^{-1}, whereas $\int(P_{u,u} + P_{v,v})\, d\sigma$ is uncorrelated with ζ. The difference in shear and normal stress–strain relations results largely from a tidal contribution in the shear component.

The difference is not simply in Brown and Owens's multiplication by a transfer function and limitation of the domain of integration to frequencies greater than $2f$. A second way of estimating the viscosity coefficient is to average $\mathrm{sgn}(S_s)C_{u,v}$, in which sgn represents the sign of its argument. Cumulative integration of the cospectrum (divided by the estimate of rms rate of strain; Fig. 3) provides a characterization of how each frequency contributes to the viscosity operator. Here, integration over $2f \le \sigma \le N$ returns horizontal viscosity estimates of about 18 m^2 s^{-1}.

Coherence estimates (Fig. 4) are about 0.05 for $\sigma > 2f$. This result is consistent with the characterization of Frankignoul (1976) that the relation between stress and horizontal rate of strain is subtle. The Brown and Owens estimate of $\nu_h = 400$ m^2 s^{-1} would imply $O(1)$ values of coherence. My estimate based on frequencies $\sigma > 2f$ differs from Brown and Owens (1981) by the number of hours in a day. I am tempted to posit an algebraic error.

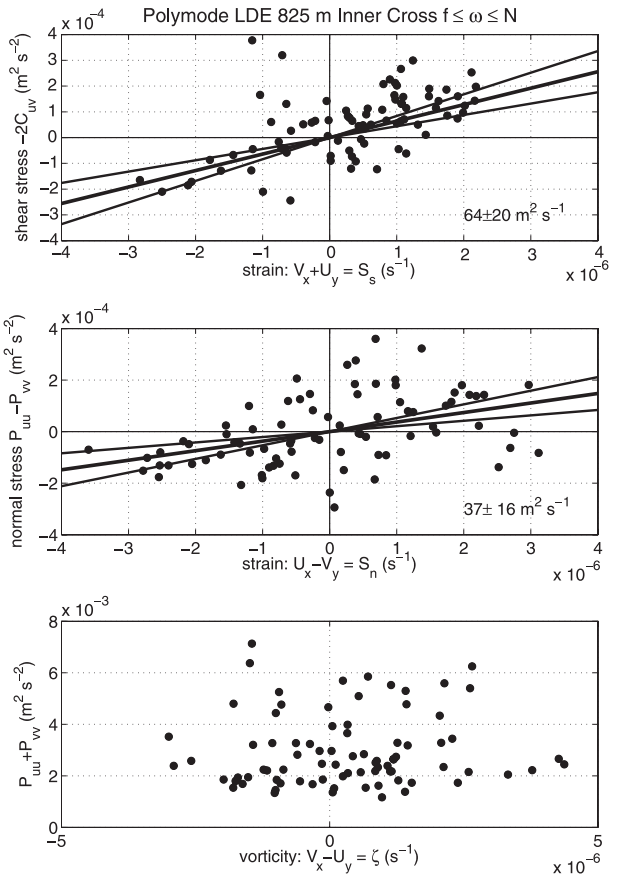

FIG. 2. (top) Scatterplots of shear stress $\int_f^N C_{u,v}\, d\omega$ against the shear component of the rate of strain S_s. (middle) Scatterplots of the normal stress $\int_f^N (P_{u,u} - P_{v,v})\, d\omega$ against the normal component of the rate of strain S_n. (bottom) Scatterplots of velocity variance $\int_f^N (P_{u,u} + P_{v,v})\, d\omega$ plotted against vorticity ζ. The regression lines of stress vs strain return horizontal viscosity coefficients of $\nu_h \cong 50$ m^2 s^{-1}. Solid dots are 10-day averages. The uncertainty estimates represent 95% confidence levels. In (bottom), no trends of kinetic energy vs relative vorticity are apparent. The lack of an apparent trend in this case is consistent with simple characterization of the coupling as a viscous process.

3. The vertical dimension

Correlations between the vertical flux of horizontal pseudomomentum and the mesoscale eddy field were pursued by Ruddick and Joyce (1979) using current meter data from PolyMode arrays I and II. For the relatively energetic moorings of the PolyMode II array, they found that (i) wave field energy levels modulated with the strength of the eddy vertical shear and (ii) there was a significant correlation between wave

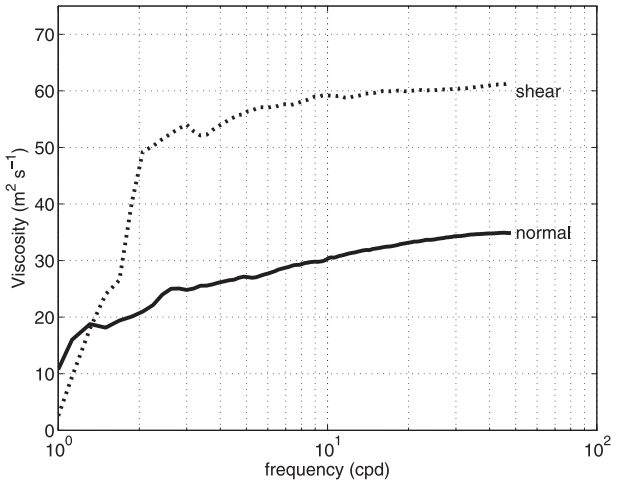

FIG. 3. Cumulative integrals of the spectral functions $-\mathrm{sgn}(S_n)[P_{u,u} - P_{v,v}]$ (thick line) and $-2\mathrm{sgn}(S_s)C_{u,v}$ (dashed line), divided by estimates of the corresponding rms rate of strain $\overline{|S_n|}$ and $\overline{|S_s|}$, to provide estimates of the horizontal viscosity ν_h.

stress and low-frequency velocity. No significant vertical stress–vertical shear correlations were apparent in either the PolyMode II data or the less energetic PolyMode I data.

Ruddick and Joyce (1979) interpret the observations as "consistent with generation of short (~1 km horizontal wavelength) internal waves by the mean shear near the thermocline, resulting in an effective viscosity of $\nu_v + (f^2/N^2)K_h \cong 0.01$ m^2 s^{-1}." Their interpretation depends on accepting the observed stresses as being significantly impacted by Doppler shifting, which in turn is consistent with the generation of internal waves from a critical layer. The less energetic moorings would be less prone to contamination by Doppler shifting, but it was perceived that the required stress–strain correlation could not be resolved there because of statistical uncertainty. This obstacle can be circumvented simply by increasing the number of degrees of freedom in the data record. Thus, the vertical coupling process was investigated here with the center, northeast, and northwest moorings of the LDE array. This provides some 995 days of data with stress–shear relations in two horizontal components from two vertically separated instruments, so that each cospectral estimate is associated with approximately 750 degrees of freedom. The eddy energy at the LDE site is comparable to the less energetic PolyMode I data and the consequent contamination of the stress estimates by mooring motion is small (Ruddick and Joyce 1979).

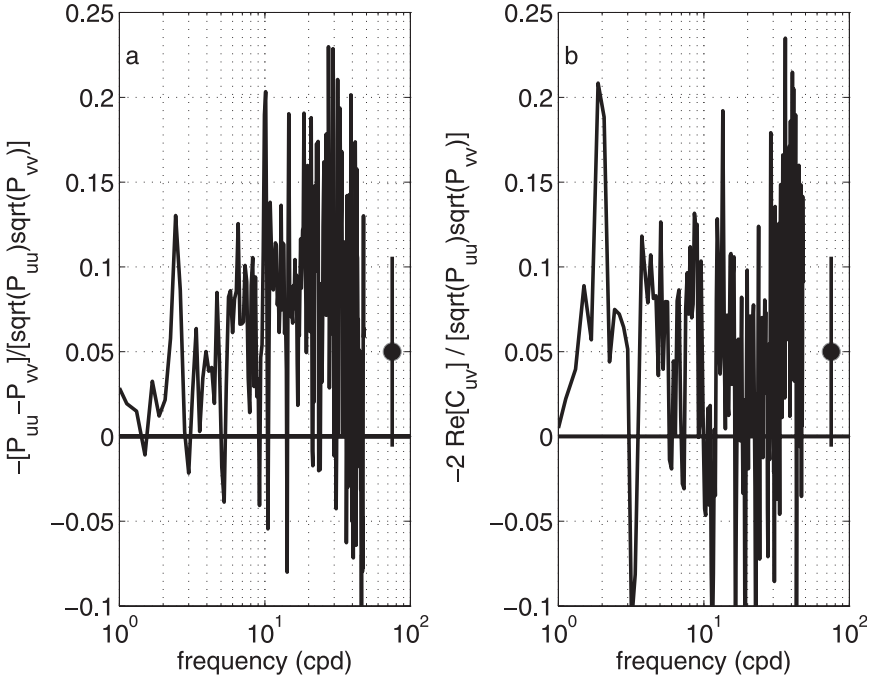

FIG. 4. Coherence functions created by averaging (a) $-\mathrm{sgn}(S_n)(P_{u,u} - P_{v,v})/P_{u,u}^{1/2}P_{v,v}^{1/2}$ and (b) $-\mathrm{sgn}(S_s)C_{u,v}/P_{u,u}^{1/2}P_{v,v}^{1/2}$ with $C_{u,v}$ being the real part of the u, v cross spectrum. Estimates are based on 1024 point transform intervals and averaging over both triangles at 825-m water depth. The symbol on the right-hand side of (a),(b) represents the standard deviation at a 0.05 coherence level with the 320 degrees of freedom expected for each cospectral estimate.

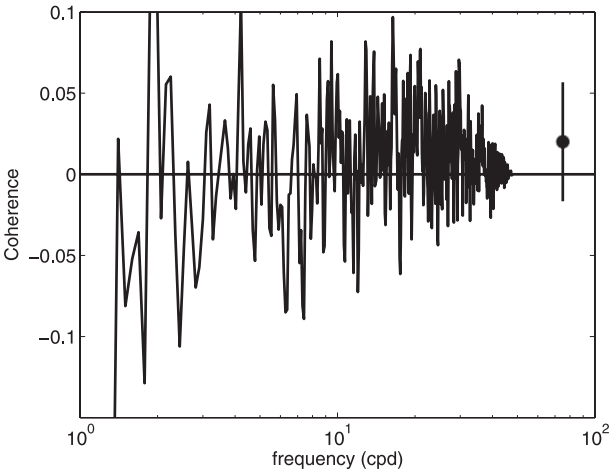

FIG. 5. Coherence function created by averaging $-\mathrm{sgn}(U_z) \times (C_{u,w} - fN^{-2}C_{v,b})/T(\omega)P_{u,u}^{1/2}P_{w,w}^{1/2}$ and $-\mathrm{sgn}(V_z)(C_{v,w} + fN^{-2}C_{u,b})/T(\omega)P_{v,v}^{1/2}P_{w,w}^{1/2}$. The factor $C_{x,y}$ represents the real part of the x, y cross spectrum. The transfer function $T(\omega) = (\omega^2 - f^2)/(\omega^2 + f^2)$ accounts for cancelation of the Reynolds stress by the buoyancy flux and renders the denominator consistent with the numerator. The coherence estimates are based on 1024 point transform intervals of data at both 600- and 825-m levels. Data are from the center, northeast, and northwest moorings. The symbol on the right-hand side of the figure represents the standard deviation at a 0.02 coherence level with the 750 degrees of freedom expected for each spectral estimate.

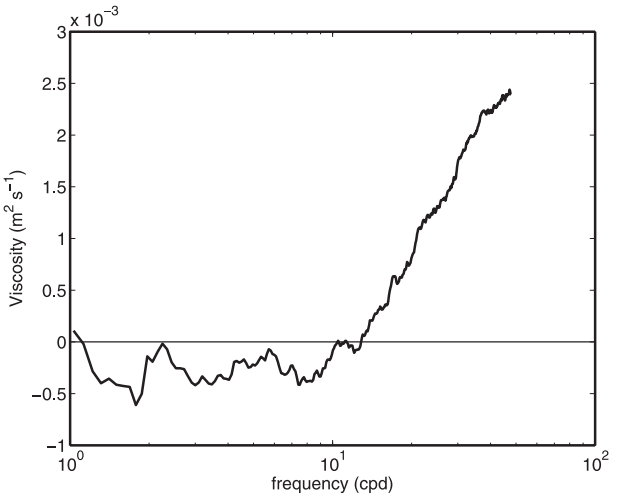

FIG. 6. Cumulative integrals of the spectral function $-\mathrm{sgn}(U_z)[(C_{u,w} - fC_{v,b})/N^2](\overline{u}_z^2)^{1/2} - \mathrm{sgn}(V_z)[(C_{v,w} - fC_{u,b})/N^2]/(\overline{v}_z^2)^{1/2}$ to provide estimates of the vertical viscosity $[\nu_v + (f^2/N^2)K_h]$. Vertical velocity was estimated by assuming a vertical balance in the temperature equation, $T_t'' + w''\overline{T}_z \cong 0$, and were corrected for the roll off associated with a center difference operator.

Evaluation of the LDE data returns a positive vertical shear–vertical stress correlation at low frequency ($\sigma < 1.2f$) and negative correlation for high frequencies ($\sigma > 10$ cph; Fig. 5). The positive stress–shear correlations at near-inertial frequencies imply the transfer of energy from the wave field to the mean, which is consistent with either critical layer or wave capture scenarios. Coherence estimates are $O(1)$ at near-inertial frequencies, but this part of the spectrum carries little effective momentum flux. Consequently, the estimates of vertical viscosity and associated energy transfer are dominated by high-frequency contributions having small coherence estimates. Integration of the cospectra returns $\nu_v + (f^2/N^2)K_h = 2.5 \pm 0.3 \times 10^{-3}$ m^2 s^{-1} (Fig. 6). The error estimate provided here represents the compounding of the nominal 750 degrees of freedom per coherence estimate (Fig. 5) over a bandwidth of 10–40 cpd containing 320 coherence estimates.

There are two landmarks of possible consequence in the frequency domain. The positive stress–shear correlation occurs for frequencies in which the wave aspect ratio is equal to or smaller than the aspect ratio of the mesoscale eddy field. The negative stress–shear correlation occurs for waves that potentially encounter a buoyancy frequency turning point: the minimum buoyancy frequency for the observed density profile is approximately 10 cpd ($N = 7 \times 10^{-4}$ s^{-1}).

4. LDE energy budgets

a. Internal wave–eddy coupling as eddy dissipation

As part of the LDE, moored current and temperature measurements were made for 15 months in the main thermocline of the Gulf Stream recirculation region near 31°N, 69°30′W to assess the energetics and dynamics of the mesoscale eddy field (Bryden 1982; Brown et al. 1986). Here, we expand slightly on the energetics documented in the study of Bryden (1982; Fig. 7).

Bryden infers a conversion of available potential energy to eddy kinetic energy at a rate of $3.3 \pm 1.7 \times 10^{-9}$ W kg^{-1} through baroclinic instability and that the mean velocity field represents a countergradient "sink" (see Fig. 1) at the rate of $1.5 \pm 0.9 \times 10^{-9}$ W kg^{-1}. The residual represents dissipation, propagation, advection, and possibly time dependence. Brown and Owens (1981) estimate that the internal wave field serves as a sink of eddy energy at a rate of $\nu_h(\overline{v}_x^2 + \overline{v}_y^2 + \overline{u}_x^2 + \overline{u}_y^2) = 1.2 \times 10^{-9}$ W kg^{-1} using $\nu_h = 200$ m^2 s^{-1} and a gradient variance estimate of 6×10^{-12} s^{-2}. Thus, approximate closure of the eddy energy budget between generation via baroclinic instability, conversion of eddy kinetic to mean kinetic energy, and interior dissipation were implied.

The estimates here of interior eddy dissipation are somewhat smaller,

$$\nu_h(\overline{v}_x^2 + \overline{v}_y^2 + \overline{u}_x^2 + \overline{u}_y^2) \cong 50\,\mathrm{m^2\,s^{-1}}\ (6 \times 10^{-12}\,\mathrm{s^{-2}})$$

$$\left(\nu_v + \frac{f^2}{N^2}K_h\right)(\overline{u}_z^2 + \overline{v}_z^2) \cong 0.0025\,\mathrm{m^2\,s^{-1}}\ (4 \times 10^{-8}\,\mathrm{s^{-2}}),$$

so that the total transfer of energy[1] from eddies to internal waves is

$$S_i = 4 \times 10^{-10}\,\mathrm{W\,kg^{-1}}.$$

Some other mechanism is required to close the eddy budget. Time dependence and propagation (through the divergence of pressure work) may play a role, and Bryden (1982) notes that the sum of baroclinic production and conversion of eddy kinetic to mean kinetic energy is smaller than the estimated uncertainty. There is, however, an obvious dissipation mechanism associated with viscous stresses in the bottom boundary layer. Standard boundary layer theory parameterizes work done against viscous stresses in the bottom boundary layer as $\rho C_D U^3$, in which U is the far-field velocity at the bottom boundary, ρ is density, and typical estimates of the drag coefficient C_D are (2–3) $\times$ 10^{-3}. The central mooring's 5332-m current meter at a height of 23 m above bottom returns an estimate of $U^3 = (\overline{u}^2 + \overline{v}^2)^{3/2} = (0.097\,\mathrm{m\,s^{-1}})^3$, which in turn implies an energy loss to viscous stress in the bottom boundary layer in the range of $1.7 < \rho C_D U^3 < 2.5$ mW m^{-2}.

A possible interpretation is that eddy energy associated with baroclinic production radiates downward through the water column and is dissipated in the bottom boundary layer. If this dissipation was distributed throughout the water column in proportion to N^2, as is the case for dissipation associated with internal wave breaking in the background internal wave field (Polzin 2004), it would be equivalent to an interior dissipation of 6–9 $\times$ 10^{-10} W kg^{-1} at 800-m depth.

This calculation, albeit based on crude extrapolation, implies that the internal wave–eddy coupling mechanism is a significant part of the total dissipation (interior plus boundary) of eddy energy. Recent demonstrations that eddy statistics in idealized quasigeostrophic turbulence models are strongly impacted by damping (Arbic and Flierl 2004; Arbic and Scott 2008) have focused on the issue of bottom dissipation.

[1] The LDE array does not fully resolve the gradient variance, but the unresolved variance is arguably acted on by a scale-dependent viscosity coefficient with consequently smaller transfer rates. These scale-dependent issues are taken up in K. L. Polzin (2009, unpublished manuscript) but do not affect the conclusions presented here regarding the energy budget.

b. *Mesoscale eddy–internal wave coupling as internal wave forcing*

If mesoscale eddy–internal wave coupling represents a sink of eddy energy, then it represents a source of internal wave energy. An open question is whether it can be considered as significant in the internal wave energy budget. The tack here is to compare the identified source rate with dissipation estimates from fine structure data obtained as part of the Frontal Air-Sea Interaction Experiment (FASINEX). Field work took place in February–March 1986 in the vicinity of an upper-ocean frontal system in the subtropical convergence zone of the northwest Atlantic (28°N, 69°W; Weller et al. 1991). Further analysis of the data appears in Polzin et al. (1996, 2003). The MODE and IWEX studies were also located here. Sampling during FASINEX took place over several degrees of latitude and longitude. It is assumed that the sampling is random relative to the underlying eddy field and so is not spatially biased. The high-frequency internal wave field in the main thermocline at 34°N, 70°W [the Long Term Upper Ocean Study (LOTUS) site] is known to exhibit an annual cycle with maximum energy in the late winter in this region (Briscoe and Weller 1984). It is not clear how this annual cycle would appear in the fine structure data, but the FASINEX data were obtained during the more energetic part of the annual cycle.

The fine structure parameterization of Polzin et al. (1995) assigns a turbulent production rate of

$$\text{production} = (1 + R_f)\epsilon_o \frac{f}{f_o}\frac{N^2}{N_o^2}E^2\sqrt{\frac{2}{R_\omega - 1}}\frac{3(R_\omega + 1)}{4R_\omega}, \tag{9}$$

where flux Richardson number $R_f = 0.15$, $\epsilon_o = 7 \times 10^{-10}$ W kg^{-1}, f_o is the Coriolis parameter at 31.5° latitude, $N_o = 3$ cph, shear spectral level E is relative to a reference of $7N^2$ (1/cpm), and the E_k–E_p ratio R_ω is estimated from vertical gradient variances. The factor $\sqrt{2/(R_\omega - 1)}$ represents a scaled aspect ratio under the hydrostatic approximation. The main thermocline fine structure observations provide the estimates $N^2 = 0.70\,N_o^2$, $E = 1.2$, and $R_\omega = 6$, which in turn imply a production of

$$\text{production}\,(z = 800\,\mathrm{m}) = 4 \times 10^{-10}\,\mathrm{W\,kg^{-1}}.$$

This represents a value numerically similar to the identified eddy forcing of the internal wave field in section 4a.

Additional dissipation of internal wave energy will be present in the bottom boundary layer. This contribution

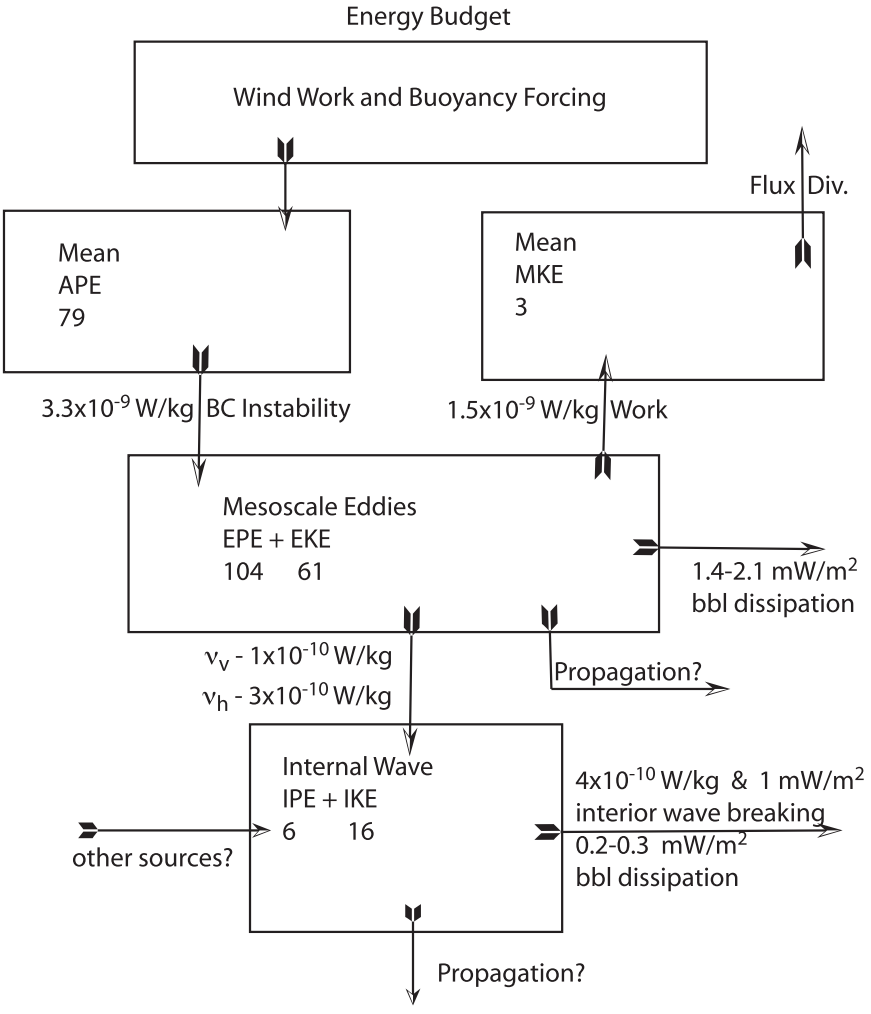

FIG. 7. A schematic of energy conversion rates derived from the LDE array, following Bryden (1982). Estimates in units of W kg^{-1} refer to energy conversions at the depths of 600–800 m. Estimates in units of W m^{-2} refer to boundary inputs or depth-integrated means. Unlabeled energy estimates are in units of 10^{-4} m^2 s^{-2}. Energy is input into the subtropical gyre by wind work and buoyancy forcing. It is converted from the mean density field (by baroclinic instability) to eddy energy. About 40% of this is converted into mean kinetic energy (Bryden 1982). The eddy field is damped by dissipation in the bottom boundary layer and forcing of the internal wave field. Bottom boundary layer dissipation may play a somewhat larger role in the eddy energy budget than interactions with the internal wave field. However, eddy–wave coupling provides a source that is in approximate balance with the estimated dissipation, implying eddy–wave coupling plays an $O(1)$ in the internal wave energy budget. With regards to the mean kinetic energy budget, Bryden (1982) finds an approximate balance between the gain associated with eddy work against the mean rate of strain and a flux divergence, $\partial_x(\overline{\bar{u}\,\overline{u'u'}} + \overline{\bar{v}\,\overline{u'v'}}) + \partial_y(\overline{\bar{u}\,\overline{u'v'}} + \overline{\bar{v}\,\overline{v'v'}})$.

to the energy budget can be quantified through a linearized formulation:

$$\text{dissipation} = 2\rho C_D |\overline{u}|(\overline{u''^2} + \overline{v''^2}).$$

With $(\overline{u''^2} + \overline{v''^2})^{1/2} = 0.025\ \text{m s}^{-1}$ being the observed near-bottom internal wave speed, the dissipation estimate becomes

$$\text{dissipation} = 0.2 - 0.3\,\text{mW m}^{-2}.$$

For comparison, dissipation in the background internal wav efield can be estimated by integrating (9) with the observed N^2 profile and amounts to a depth-integrated dissipation of 1 mW m^{-2}. The estimated forcing through wave–eddy coupling is the same order of magnitude as the anticipated dissipation. Application of this fine structure

parameterization scheme to Absolute Velocity Profiler (AVP) data obtained during the PolyMode LDE (Kunze and Sanford 1996) returns similar results.

With caveats about this being a crude extrapolation and with knowledge that the upper-ocean frontal regime present in this region (Weller et al. 1991; Polzin et al. 1996) represents an ill-defined departure from the stated assumptions in the extrapolation used to define both sources and sinks, I conclude that the mesoscale eddy–internal wave coupling is a dominant energy source for the internal wave field in the Gulf Stream recirculation.

5. Summary

Current meter array data from the LDE of the PolyMode field program were used in investigate the coupling of the mesoscale eddy and internal wave fields in the southern recirculation gyre of the Gulf Stream. The coupling was characterized as a viscous process. Viscosity coefficients inferred from regressions of horizontal stress versus horizontal rate of strain return estimates of $\nu_h = 64 \pm 20$ m^2 s^{-1} and $\nu_h = 37 \pm 16$ m^2 s^{-1}. The regression of effective vertical stress estimates against vertical shear returns $\nu_v + (f^2/N^2)K_h = 2.5 \pm 0.3 \times 10^{-3}$ m^2 s^{-1}. In terms of energy budgets, eddy–wave coupling represents a significant mechanism by which eddy energy is dissipated and plays an $O(1)$ role in the energy budget of the internal wave field.

These results may be specific to the LDE region, which is situated at the exit of the southern recirculation gyre. Variability of the viscosity coefficients acting on the mesoscale field will depend on variability in the background wave field. Such variability exists (Polzin and Lvov 2009, manuscript submitted to *Rev. Geophys.*). A possible implication of this work is that the variability in both the mesoscale eddy field (Zang and Wunsch 2001) and the internal wave field (Polzin and Lvov 2009, manuscript submitted to *Rev. Geophys.*) are related through mesoscale eddy–internal wave coupling. In terms of understanding the geographic variability of viscosity coefficients, there is a simplicity if the energetics of the internal wave field are dominated by an interior coupling to the mesoscale eddy field, as appears to be the case in the southern recirculation gyre. This represents the dynamic balance advocated by Müller and Olbers (1975), albeit at somewhat reduced interaction rates.

This study comes with many caveats:

- The maximum observational record length for the LDE array data is 15 months, but the failure of certain instruments reduces the usable record length to 225 days. Stable estimates of time-mean quantities typically require averaging periods on the order of 500 days (Schmitz 1977). The mean quantities quoted here represent record length means with associated record length uncertainties. See Bryden (1982) and Brown et al. (1986) for further discussion of these uncertainties. I note, however, that the available 15-month estimates are consistent with the 225-day record means (to within uncertainty). Any differences do not change the interpretation presented here.
- The LDE array does not fully spatially resolve the mesoscale eddy velocity gradient variances. This issue is examined in the companion manuscript where resolution of the enstrophy gradient variance is even more problematic. Again, consideration of such issues does not change the interpretation presented here.
- The characterization of the coupling through a flux–gradient relation applies only to quasigeostrophic flows in which the flow field is horizontally nondivergent to O(Rossby number squared). Symmetric flow structures such as rings and jets are not coupled in the same manner.
- The interpretive paradigm being pursued here and in related work (Polzin 2008; K. L. Polzin 2009, unpublished manuscript) is one of wave propagation in a horizontally nondivergent mesoscale eddy velocity field in which exchanges of energy and momentum are rendered permanent through wave damping or nonlinearity. Wave propagation is assumed to be consistent with ray tracing and action conservation, which in turn assumes a scale separation between wave and background and that the wave amplitude is small relative to the background. These assumptions are harmonious with (i) an enstrophy cascade regime of quasigeostrophic turbulence in which energy spectra roll off as k_h^{-3} and (ii) observed acceleration spectra (Rupolo et al. 1996) from the main thermocline of the western North Atlantic, which suggest a slightly steeper $k_h^{-3.3}$ spectral slope for the eddy energy spectrum. Potential vorticity containing motions on horizontal scales of 1–10 km are quite difficult to measure, however, and such acceleration spectra do not preclude the presence of vortical modes associated with generation via topographic torques (Kunze and Sanford 1993) or internal wave breaking (Polzin et al. 2003; Polzin and Ferrari 2004). Part of the difficulty is that internal waves will tend to dominate the velocity field at horizontal wavelengths smaller than 100 km, which conflicts with the small-amplitude approximation. Finally, the focus here has been on interpreting observations from the main thermocline. Altimeter data exhibit much shallower spectral slopes in energetic western boundary current regimes, closely following a $k_h^{-5/3}$ spectrum that has been interpreted as an energy cascade associated with surface quasigeostrophic

dynamics (LeTraon et al. 2008). Thus, the upper ocean may not fit nicely into the interpretive paradigm being pursued here. Alternative interpretive paradigms are presented in Ford et al. (2000; Lighthill radiation), Klein et al. (2004; near-inertial oscillation dynamics), and Riley and Lelong (2000; nonlinear wave–vortex interactions/rotating stratified turbulence).

6. Discussion

The discussion here tries to flesh out some of the broader implications of eddy–wave coupling as they appear in the context of the PolyMode field program.

a. Coherent vortices

One of the surprises of the Local Dynamics Experiment was the prevalence of coherent submesoscale lenses (Elliot and Sanford 1986a). These lenses typically had temperature–salinity properties that distinguished them as having relatively long (several years) life spans. These submesoscale features had horizontal scales of $L = 15$ km, significantly smaller than the mesoscale field ($\cong$100 km). Such life spans are not consistent with a viscous decay and $\nu_h = 50\ \mathrm{m^2\ s^{-1}}$, which provides a temporal spin-down scale $L^2/\nu_h \cong$ of 50 days.

However, note that the relative vorticity variance in the core of such lenses (Elliot and Sanford 1986b) dominates the rate of strain variance, so by the criterion (5) one does not expect a strong coupling between the internal wave field and the mesoscale eddy field. Moreover, as a symmetric feature, the assumptions leading to a flux–gradient relation are not valid and the expectations of a short temporal spin-down scale are incorrect. The viscosity operators here are appropriate for a three-dimensional field (Fig. 1a), not two-dimensional fields (Fig. 1b).

A viscous closure cannot be anticipated from analytic results with axisymmetric (e.g., zonal) flows. In that instance, apart from diabatic processes or critical layers, the pseudomomentum flux is nondivergent. Extrapolation of this result to nonaxisymmetric background flows gives the misleading impression that the only consequence of internal waves for geostrophically balanced flows is through a diabatic link. The existence of long-lived, coherent submesoscale vortices is consistent with the proposed model of wave–eddy interaction.

b. Topographic Rossby waves

Price and Rossby (1982) document that the subthermocline velocity field at the start of the LDE is dominated by highly polarized oscillatory flow that is consistent with topography Rossby wave characteristics: the horizontal wavelength (340 km), intrinsic frequency (1/61 cpd), and phase propagation toward 300°T agree with a the dispersion relation of barotropic planetary waves modified by topography. The group velocity is approximately $0.05\ \mathrm{m\ s^{-1}}$ directed toward 100°T (eastward). The LDE was situated at the exit of the southern recirculation gyre, and the mean rate of strain is nonzero. This topographic wave is oriented so that energy is being transferred from the wave to the mean field (Fig. 1). Such events dominate the record length estimates of energy transfer in Bryden (1982).

A large part of the mesoscale eddy field at the LDE site is linear waves, and the energetic transfer estimates of Bryden (1982) fit nicely into a wave–mean interaction paradigm described in section 1c. However, this statement comes with major caveats. Observed particle speeds ($0.12\ \mathrm{m\ s^{-1}}$) exceed the phase speed by about a factor of 2.

c. Vertical mode coupling

A second caveat regarding nonlinearity is that planetary wave fits to the mesoscale eddy field require a superposition of several barotropic and baroclinic plane waves to match the horizontal structure of the observed velocity field (Hua et al. 1986). The vertical modes are dynamically coupled and the potential vorticity balance of the baroclinic mode has significant nonlinear contributions, especially at the smallest resolved scales. Of two interaction events, one is described as the straining of an antecedent, large-scale baroclinic flow into a baroclinic jet by the barotropic wave described earlier. Although the interpretation offered in Hua et al. (1986) is based on nonlinearity, the role of internal waves in contributing to the baroclinic jet through a frontogenetic process is an alternative hypothesis that has yet to be explored.

Acknowledgments. Much of the intellectual content of this paper evolved out of discussions with R. Ferrari. The manuscript benefited from discussions with Brian Arbic and Rob Scott and a review provided by Peter Rhines. Salary support for this analysis was provided by Woods Hole Oceanographic Institution bridge support funds.

REFERENCES

Andrews, D. G., and M. E. McIntyre, 1976: Planetary waves in horizontal and vertical shear: The generalized Eliassen-Palm relation and the mean zonal acceleration. *J. Atmos. Sci.,* **33,** 2031–2048.

——, J. R. Holton, and C. B. Leovy, 1987: *Middle Atmosphere Dynamics*. Academic Press, 489 pp.

Arbic, B. K., and G. R. Flierl, 2004: Baroclinically unstable geostrophic turbulence in the limits of strong and weak bottom Ekman friction: Application to mid-ocean eddies. *J. Phys. Oceanogr.,* **34,** 2257–2273.

——, and R. B. Scott, 2008: On quadratic bottom drag, geostrophic turbulence, and oceanic mesoscale eddies. *J. Phys. Oceanogr.,* **38,** 84–103.

Briscoe, M. G., and R. A. Weller, 1984: Preliminary results from the long-term upper-ocean study (LOTUS). *Dyn. Atmos. Oceans,* **8,** 243–265.

Brown, E. D., and W. B. Owens, 1981: Observations of the horizontal interactions between the internal wave field and the mesoscale flow. *J. Phys. Oceanogr.,* **11,** 1474–1480.

——, ——, and H. L. Bryden, 1986: Eddy-potential vorticity fluxes in the Gulf Stream recirculation. *J. Phys. Oceanogr.,* **16,** 523–531.

Bryden, H. L., 1982: Sources of eddy energy in the Gulf Stream recirculation region. *J. Mar. Res.,* **40,** 1047–1068.

Bühler, O., and M. E. McIntyre, 2005: Wave capture and wave-vortex duality. *J. Fluid Mech.,* **534,** 67–95.

Elliot, B. A., and T. B. Sanford, 1986a: The subthermocline lens D1. Part I: Description of water properties and the velocity profiles. *J. Phys. Oceanogr.,* **16,** 532–548.

——, and ——, 1986b: The subthermocline lens D1. Part II: Kinematics and dynamics. *J. Phys. Oceanogr.,* **16,** 549–561.

Ferrari, R., and C. Wunsch, 2009: Ocean circulation kinetic energy—Reservoirs, sources and sinks. *Annu. Rev. Fluid Mech.,* **41,** 253–282.

Ford, R., M. E. McIntyre, and W. A. Norton, 2000: Balance and the slow quasimanifold: Some explicit results. *J. Atmos. Sci.,* **57,** 1236–1254.

Frankignoul, C., 1974: Observed anisotropy of spectral characteristics of internal waves induced by low-frequency currents. *J. Phys. Oceanogr.,* **4,** 625–634.

——, 1976: Observed interaction between oceanic internal waves and mesoscale eddies. *Deep-Sea Res.,* **23,** 805–820.

——, and T. M. Joyce, 1979: On the internal wave variability during the internal wave experiment (IWEX). *J. Geophys. Res.,* **84,** 769–776.

Hua, B. L., J. C. McWilliams, and W. B. Owens, 1986: An objective analysis of the POLYMODE Local Dynamics Experiment. Part II: Streamfunction and potential vorticity fields during the intensive period. *J. Phys. Oceanogr.,* **16,** 506–522.

Jones, W. L., 1969: Ray tracing for internal gravity waves. *J. Geophys. Res.,* **74,** 2028–2033.

Klein, P., S. L. Smith, and G. Lapeyre, 2004: Organization of near-inertial energy by an eddy field. *Quart. J. Roy. Meteor. Soc.,* **130,** 1153–1166.

Kunze, E., and T. B. Sanford, 1993: Submesoscale dynamics near a seamount. Part I: Measurements of Ertel vorticity. *J. Phys. Oceanogr.,* **23,** 2567–2588.

——, and ——, 1996: Abyssal mixing: Where it is not. *J. Phys. Oceanogr.,* **26,** 2286–2296.

LeTraon, P. Y., P. Klein, and B. L. Hua, 2008: Do altimeter wavenumber spectra agree with the interior or surface quasi-geostrophic theory? *J. Phys. Oceanogr.,* **38,** 1137–1142.

Moore, D. W., 1963: Rossby waves in ocean circulation. *Deep-Sea Res.,* **10,** 735–748.

Müller, P., 1976: On the diffusion of momentum and mass by internal gravity waves. *J. Fluid Mech.,* **77,** 789–823.

——, and D. J. Olbers, 1975: On the dynamics of internal waves in the deep ocean. *J. Geophys. Res.,* **80,** 3848–3860.

Munk, W., 1950: On the wind-driven circulation. *J. Meteor.,* **7,** 79–93.

Polzin, K. L., 2004: A heuristic description of internal wave dynamics. *J. Phys. Oceanogr.,* **34,** 214–230.

——, 2008: Mesoscale eddy–internal wave coupling. Part I: Symmetry, wave capture and results from the Mid-Ocean Dynamics Experiment. *J. Phys. Oceanogr.,* **38,** 2556–2574.

——, and R. Ferrari, 2004: Isopycnal dispersion in nature. *J. Phys. Oceanogr.,* **34,** 247–257.

——, J. M. Toole, and R. W. Schmitt, 1995: Finescale parameterizations of turbulent dissipation. *J. Phys. Oceanogr.,* **25,** 306–328.

——, N. S. Oakey, J. M. Toole, and R. W. Schmitt, 1996: Fine structure and microstructure characteristics across the northwest Atlantic Subtropical Front. *J. Geophys. Res.,* **101,** 14 111–14 121.

——, E. Kunze, J. M. Toole, and R. W. Schmitt, 2003: The partition of fine-scale energy into internal waves and subinertial motions. *J. Phys. Oceanogr.,* **33,** 234–248.

Price, J. F., and H. T. Rossby, 1982: Observations of a barotropic planetary wave in the western North Atlantic. *J. Mar. Res.,* **40** (Suppl.), 543–558.

Provenzale, A., 1999: Transport by coherent barotropic vortices. *Annu. Rev. Fluid Mech.,* **31,** 55–93.

Riley, J. J., and M.-P. Lelong, 2000: Fluid motions in the presence of strong stable stratification. *Annu. Rev. Fluid Mech.,* **32,** 613–658.

Ruddick, B. R., and T. M. Joyce, 1979: Observations of interaction between the internal wavefield and low-frequency flows in the North Atlantic. *J. Phys. Oceanogr.,* **9,** 498–517.

Rupolo, V., B. L. Hua, A. Provenzale, and V. Artale, 1996: Lagrangian velocity spectra at 700 m in the western North Atlantic. *J. Phys. Oceanogr.,* **26,** 1591–1607.

Schmitz, W. J., 1976: A comparison of the mid-latitude eddy fields in the western North Atlantic and North Pacific Oceans. *J. Phys. Oceanogr.,* **12,** 208–210.

——, 1977: On the deep general circulation in the western North Atlantic. *J. Mar. Res.,* **35,** 21–28.

Shepherd, T. G., 1990: Symmetries, conservation laws, and Hamiltonian structure in geophysical fluid dynamics. *Advances in Geophysics,* Vol. 32, Academic Press, 287–338.

Starr, V. P., 1968: *Physics of Negative Viscosity Phenomena*. McGraw-Hill, 256 pp.

Stommel, H., 1948: The westward intensification of wind-driven ocean currents. *Trans. Amer. Geophys. Union,* **29,** 202–206.

Tennekes, H., and J. L. Lumley, 1972: *A First Course in Turbulence*. MIT Press, 300 pp.

Weller, R. A., D. L. Rudnick, C. C. Eriksen, K. L. Polzin, N. S. Oakey, J. M. Toole, R. W. Schmitt, and R. T. Pollard, 1991: Forced ocean response during the Frontal Air-Sea Interaction Experiment. *J. Geophys. Res.,* **96,** 8611–8693.

Wunsch, C., and R. Ferrari, 2004: Vertical mixing, energy, and the general circulation of the oceans. *Annu. Rev. Fluid Mech.,* **36,** 281–314.

Zang, X., and C. Wunsch, 2001: Spectral description of low-frequency oceanic variability. *J. Phys. Oceanogr.,* **31,** 3073–3095.